Journal of Solid State Chemistry 182 (2009) 2632–2639

Contents lists available at ScienceDirect

Journal of Solid State Chemistry

journal homepage: www.elsevier.com/locate/jssc

Neutron powder diffraction and difference maximum entropy method analysis of protium- and deuterium-dissolved $BaSn_{0.5}In_{0.5}O_{2.75+\alpha}$

Takanori Nagasaki [a,*], Shinya Shiotani [b], Naoki Igawa [c], Masahito Yoshino [b], Kouta Iwasaki [b], Hiroshi Fukazawa [c], Wataru Utsumi [c]

[a] EcoTopia Science Institute, Nagoya University, Nagoya 464-8603, Japan
[b] Graduate School of Engineering, Nagoya University, Nagoya 464-8603, Japan
[c] Quantum Beam Science Directorate, Japan Atomic Energy Agency, Tokai-mura, Ibaraki 319-1195, Japan

ARTICLE INFO

Article history:
Received 9 March 2009
Received in revised form
10 June 2009
Accepted 17 June 2009
Available online 23 June 2009

Keywords:
Neutron diffraction
Maximum entropy method
Proton conductor
Perovskite oxide
$BaSn_{0.5}In_{0.5}O_{2.75}$

ABSTRACT

We propose a new method, a difference maximum entropy method (MEM) analysis of the neutron diffraction data, for revealing the detailed structure around hydrogen atoms in proton-conducting oxides. This MEM analysis uses the differences between the structure factors of protium- and deuterium-dissolved crystals. Simulations demonstrate that it not only provides the distribution of hydrogen atoms alone, but also improves the spatial resolution of MEM mapping around hydrogen atoms. Applied to actual diffraction data of protium- and deuterium-dissolved $BaSn_{0.5}In_{0.5}O_{2.75+\alpha}$ at 9 K, difference MEM analysis reveals that O–D bonds mostly tilt towards the second nearest oxygen atoms, and that the distributions of deuterium and oxygen atoms are probably insignificant in interstitial regions.

1. Introduction

Some perovskite oxides with dopant cations and oxide ion vacancies absorb water vapor in a humid atmosphere to release mobile hydrogen ions (protons) into the structure, thereby becoming proton conductors. $BaZr_{1-x}M_xO_{3-x/2}$, $BaCe_{1-x}M_xO_{3-x/2}$, and $SrCe_{1-x}M_xO_{3-x/2}$ (M: dopant) are examples of this class of materials. These materials are not only of fundamental interest, but also of practical interest because of their potential application to protonic devices including fuel cells [1].

In previous studies, we performed neutron powder diffraction experiments on D_2O-dissolved $BaSn_{0.5}In_{0.5}O_{2.75}$ at 10–473 K [2,3], and D_2O-dissolved $BaZr_{0.5}In_{0.5}O_{2.75}$ at 10 K [4]. Analyzing the data by the Rietveld method and the maximum entropy method (MEM), we found that the deuterium atoms were located at, or close to, the 12h site in the Wyckoff notation of the cubic perovskite structure (space group $Pm\bar{3}m$, see Fig. 1). In other words, the O–H bond was directed (roughly) along the bisector of the edges of the adjacent MO_6 (M: Sn, Zr, In) octahedra. (We refer to such a hydrogen site as a bisector site.)

Recently, using neutron powder diffraction, Ahmed et al. [6], Kendrick et al. [7], and Azad et al. [8] found that hydrogen atoms occupied the bisector site in $BaZr_{0.5}In_{0.5}O_{3-y}$ at 5 K, $La_{0.73}Ba_{0.27}ScO_{2.865}-0.135(H/D)_2O$ at 4.2 K, and $BaCe_{0.4}Zr_{0.4}Sc_{0.2}O_{2.90}-0.10D_2O$ at 5–500 K, respectively. Some computational studies [9–16] for similar materials also suggested the bisector site as a hydrogen atom position. These results indicate that the occupation of the bisector site by hydrogen atoms is common in many proton-conducting perovskite oxides.

However, there are still questions about the detailed structure around hydrogen atoms in $BaSn_{0.5}In_{0.5}O_{2.75+\alpha}$ and $BaZr_{0.5}In_{0.5}O_{2.75+\alpha}$, because the results of the Rietveld and MEM analyses were somewhat inconsistent [2–4]. The Rietveld analysis showed that the deuterium atoms in $BaSn_{0.5}In_{0.5}O_{2.75+\alpha}$ were located at the 48n site, slightly off the {100} planes; the O–D bonds tilted towards the oxygen atoms second nearest to the deuterium atoms. On the other hand, the MEM analysis using the structure factors determined by the Rietveld analysis showed that deuterium atoms were distributed around the 12h site on the {100} planes; there were few, if any, O–D bonds that tilted towards the second nearest oxygen atoms. In addition, the MEM analysis yielded small, yet finite, scattering length density between the normal sites of oxygen and deuterium. It appeared that a significant number of oxygen and/or deuterium atoms deviated from their normal sites to be distributed over the interstitial regions.

Both the O–H tilting suggested by the Rietveld analysis and the O/H deviation suggested by the MEM analysis can be attributed, at

* Corresponding author. Fax: +81 52 789 5158.
E-mail address: nagasaki@esi.nagoya-u.ac.jp (T. Nagasaki).

0022-4596/$ - see front matter © 2009 Elsevier Inc. All rights reserved.
doi:10.1016/j.jssc.2009.06.024

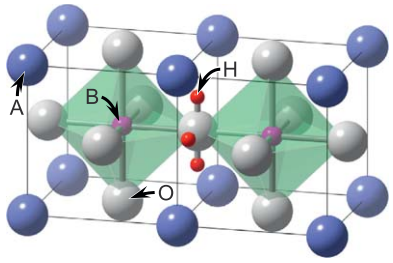

Fig. 1. Hydrogen atoms at the 12*h* (0, *y*, 0.5) site of a cubic perovskite oxide ABO_3 (space group $Pm\bar{3}m$). Our previous studies [2–4] revealed that deuterium atoms in D_2O-dissolved $BaSn_{0.5}In_{0.5}O_{2.75}$ (10–473 K) and D_2O-dissolved $BaZr_{0.5}In_{0.5}O_{2.75}$ (10 K) are located at, or close to, the 12*h* site with an O–D distance of 0.9–1.0 Å. We refer to such a hydrogen site as a bisector site. (The drawings in Figs. 1–3 and 5 were made using the program VESTA [5].)

least qualitatively, to asymmetric local environments arising from charged defects such as dopant cations and/or oxygen vacancies [14,17]. They are often accompanied by the formation of hydrogen bonds between the hydrogen atoms and the second nearest oxygen atoms [14]. These hydrogen bonds will help hydrogen atoms jump between oxygen atoms; on the other hand, they will hinder the rotation of hydrogen atoms around oxygen atoms. In other words, they have the opposing effects of enhancing and suppressing hydrogen diffusion. Thus it is important to elucidate the detailed structure around the hydrogen atoms to understand the hydrogen diffusion mechanism.

Recently, MEM has been used to investigate static and dynamic disorder in ionic conductors [18], and so one might think that the result of the MEM analysis is more reliable than that of the Rietveld analysis. However, the results of our MEM analysis seemed to suffer from the relatively long wavelength (182.3 pm) of the neutrons used in the experiments [4]. This leads to a lack of data for a *d*-spacing less than 90–100 pm and limits the spatial resolution of the three-dimensional map deduced by MEM for scattering length density distribution.

The most straightforward approach to improve the spatial resolution is to use shorter wavelength neutrons. Actually, neutrons with a wavelength of 116.3 pm are also available at the diffractometer we used (high resolution powder diffractometer (HRPD), Japan Atomic Energy Agency). However, their flux density is an order of magnitude smaller than that of 182.3 pm neutrons, making experiments using them rather impractical.

Therefore, in the present paper, we propose a new method that we call difference MEM analysis, which uses the differences between the structure factors of protium- and deuterium-dissolved crystals. After describing basic equations for difference MEM analysis, we demonstrate by simulation that it effectively improves the spatial resolution of MEM mapping around hydrogen atoms as well as provides the distribution of hydrogen atoms alone. We then apply it to the actual neutron diffraction data of protium- and deuterium-dissolved $BaSn_{0.5}In_{0.5}O_{2.75+\alpha}$, and discuss hydrogen distribution in it.

2. Analysis methods

2.1. Basic equations for difference MEM analysis

Let us consider protium- and deuterium-dissolved, but otherwise identical, crystals. The structure factors of these crystals are

$$F_1(\boldsymbol{h}_K) = \int_V \rho_1(\boldsymbol{r})\exp(2\pi i\boldsymbol{h}_K\cdot\boldsymbol{r})d\boldsymbol{r} = \int_V [\rho_H(\boldsymbol{r}) + \rho'(\boldsymbol{r})]\exp(2\pi i\boldsymbol{h}_K\cdot\boldsymbol{r})\,d\boldsymbol{r}, \quad (1)$$

and

$$F_2(\boldsymbol{h}_K) = \int_V \rho_2(\boldsymbol{r})\exp(2\pi i\boldsymbol{h}_K\cdot\boldsymbol{r})d\boldsymbol{r} = \int_V [\rho_D(\boldsymbol{r}) + \rho'(\boldsymbol{r})]\exp(2\pi i\boldsymbol{h}_K\cdot\boldsymbol{r})\,d\boldsymbol{r}, \quad (2)$$

respectively, where $\rho_H(\boldsymbol{r})$, $\rho_D(\boldsymbol{r})$, and $\rho'(\boldsymbol{r})$ are the neutron scattering length densities at a point $\boldsymbol{r}$ due to protium atoms, deuterium atoms and other constituent atoms, respectively; $\boldsymbol{h}_K$ is a reciprocal lattice vector and V means the integration is done over the unit cell volume. Here we assume that the distributions of the protium and deuterium atoms are the same, namely

$$\frac{\rho_H(\boldsymbol{r})}{b_H} = (n_H(\boldsymbol{r}) = n_D(\boldsymbol{r}) =)\frac{\rho_D(\boldsymbol{r})}{b_D}, \quad (3)$$

where b_H and b_D are the respective coherent neutron scattering lengths of protium and deuterium, and $n_H(\boldsymbol{r})$ and $n_D(\boldsymbol{r})$ are the respective number densities of protium and deuterium atoms at $\boldsymbol{r}$.

We define a set of difference structure factors as

$$\Delta F_D(\boldsymbol{h}_K) \equiv \frac{b_D[F_2(\boldsymbol{h}_K) - F_1(\boldsymbol{h}_K)]}{b_D - b_H} = \int_V \rho_D(\boldsymbol{r})\exp(2\pi i\boldsymbol{h}_K\cdot\boldsymbol{r})\,d\boldsymbol{r}, \quad (4)$$

which reflect the scattering length density distribution $\rho_D(\boldsymbol{r})$ of deuterium atoms alone. When the structure factors are experimentally determined, errors in the difference structure factors are evaluated via the error propagation law,

$$\sigma_D(|\Delta F_D(\boldsymbol{h}_K)|) \equiv \frac{b_D\sqrt{[\sigma_1(|F_1(\boldsymbol{h}_K)|)]^2 + [\sigma_2(|F_2(\boldsymbol{h}_K)|)]^2}}{b_D - b_H}, \quad (5)$$

where $\sigma(|F(\boldsymbol{h}_K)|)$ are the errors in the structure factors $F(\boldsymbol{h}_K)$. Through MEM analysis of the experimentally determined $\Delta F_D(\boldsymbol{h}_K)$ with $\sigma_D(|\Delta F_D(\boldsymbol{h}_K)|)$, we can obtain the scattering length density distribution of deuterium (hydrogen) atoms alone. We refer to this procedure as difference MEM analysis.

We define another set of difference structure factors as

$$\Delta F'(\boldsymbol{h}_K) \equiv \frac{b_D F_1(\boldsymbol{h}_K) - b_H F_2(\boldsymbol{h}_K)}{b_D - b_H} = \int_V \rho'(\boldsymbol{r})\exp(2\pi i\boldsymbol{h}_K\cdot\boldsymbol{r})\,d\boldsymbol{r}, \quad (6)$$

which reflect the neutron scattering length density distribution $\rho'(\boldsymbol{r})$ of constituent atoms excluding hydrogen atoms. Their errors are

$$\sigma'(|\Delta F'(\boldsymbol{h}_K)|) \equiv \frac{\sqrt{[b_D\sigma_1(|F_1(\boldsymbol{h}_K)|)]^2 + [b_H\sigma_2(|F_2(\boldsymbol{h}_K)|)]^2}}{b_D - b_H}. \quad (7)$$

The experimentally determined $\Delta F'(\boldsymbol{h}_K)$ and $\sigma'(|\Delta F'(\boldsymbol{h}_K)|)$ allow us to deduce the scattering length density distribution of constituent atoms excluding hydrogen atoms by MEM analysis.

Moreover, we can obtain the total scattering length density distribution as

$$\rho_{D,MEM}(\boldsymbol{r}, \Delta F_D(\boldsymbol{h}_K), \sigma_D(|\Delta F_D(\boldsymbol{h}_K)|)) + \rho'_{MEM}(\boldsymbol{r}, \Delta F'(\boldsymbol{h}_K), \sigma'(|\Delta F'(\boldsymbol{h}_K)|)), \quad (8)$$

where $\rho_{MEM}(\boldsymbol{r}, F(\boldsymbol{h}_K), \sigma(|F(\boldsymbol{h}_K)|))$ is the scattering length density at $\boldsymbol{r}$ deduced by MEM from the structure factors $F(\boldsymbol{h}_K)$ and their errors $\sigma(|F(\boldsymbol{h}_K)|)$. We refer to this procedure as combined difference MEM analysis, or simply as difference MEM analysis in its wider meaning. It should be noted that

$$\rho_{D,MEM}(\boldsymbol{r}, \Delta F_D(\boldsymbol{h}_K), \sigma_D(|\Delta F_D(\boldsymbol{h}_K)|)) + \rho'_{MEM}(\boldsymbol{r}, \Delta F'(\boldsymbol{h}_K), \sigma'(|\Delta F'(\boldsymbol{h}_K)|)) \neq \rho_{2,MEM}(\boldsymbol{r}, F_2(\boldsymbol{h}_K), \sigma_2(|F_2(\boldsymbol{h}_K)|)) \quad (9)$$

although

$$\Delta F_D(\boldsymbol{h}_K) + \Delta F'(\boldsymbol{h}_K) = F_2(\boldsymbol{h}_K). \quad (10)$$

In other words, the combined difference MEM analysis and the ordinary MEM analysis do *not* yield the same results despite being based on the same structure factors. As shown later by simulations, the former has higher effective spatial resolution in MEM mapping around hydrogen atoms. This feature is not found in "difference" Fourier synthesis, and is the main feature of difference MEM analysis.

In the above argument, we have assumed that there is no isotope effect in the hydrogen distribution. However, an isotope effect does exist in hydrogen vibration. It has been reported [14,19] that the protium atoms in the proton-conducting perovskite oxides are bound to oxygen atoms and vibrate at stretching frequencies corresponding to 2000–4000 cm^{-1}. For these vibration modes, virtually all the hydrogen atoms are in the ground state below room temperature because

$$kT/(\hbar\omega) \lesssim 0.1 \ll 1 \quad (11)$$

even at 300 K; here k is the Boltzmann constant, T the temperature, ω the angular frequency, and $\hbar = h/(2\pi)$ with h being the Planck constant. If we consider the stretching vibration as one dimensional harmonic oscillation, the root mean square displacement (RMSD) of the zero-point vibration is given by

$$\sqrt{\langle x^2 \rangle} = \sqrt{\hbar/(2m\omega)}, \quad (12)$$

where m is the mass of a hydrogen atom. It follows that the RMSDs of protium atoms for 2000 cm^{-1} vibration and deuterium atoms for $2000/2^{1/2}$ cm^{-1} vibration are 9.1 and 7.7 pm, respectively. This difference is likely to be smaller than the atomic displacement due to the local structural disorder in $BaSn_{0.5}In_{0.5}O_{2.75}$ (see the atomic displacement parameters U in Table 1); thus we could neglect the isotope effect in the hydrogen distribution resulting from the hydrogen vibration in this particular case.

Table 1
Crystal structure parameters and R factors for H_2O- and D_2O-dissolved $BaSn_{0.5}In_{0.5}O_{2.75}$ at 9 K determined by Rietveld analysis.

Sample	$BaSn_{0.5}In_{0.5}O_{2.75}-0.188H_2O$	$BaSn_{0.5}In_{0.5}O_{2.75}-0.188D_2O$
Space group	$Pm\bar{3}m$	$Pm\bar{3}m$
Z	1	1
a (Å)	4.1892(1)	4.1886(1)
Atom	Ba	Ba
Site	1a	1a
g	1	1
x ($= y = z$)	0	0
U_{iso} (Å^2)	0.0163(3)	0.0166(3)
Atom	Sn/In	Sn/In
Site	1b	1b
g	1	1
x ($= y = z$)	1/2	1/2
U_{iso} (Å^2)	0.0087(4)	0.0097(3)
Atom	O	O
Site	3c	3c
g	0.979[a]	0.979[a]
x ($= y$)	1/2	1/2
z	0	0
U_{11} ($= U_{22}$) (Å^2)	0.0213(4)	0.0230(4)
U_{33} (Å^2)	0.0114(7)	0.0114(5)
Atom	H	D
Site	12h	48h
g	0.0314[a]	0.0078[a]
x	0	0.067(3)
y	0.208(5)	0.285(3)
z	1/2	0.444(3)
U_{iso} (Å^2)	0.062(7)	0.003(4)
d_{O-H} or d_{O-D} (Å)	1.22(2)	0.97(1)
R_{wp} (%)	3.47	4.59
R_e (%)	3.27	4.30
R_B (%)	1.18	1.16
R_F (%)	0.70	0.72
S ($\equiv R_{wp}/R_e$)	1.06	1.07

[a] Determined by thermogravimetry.

2.2. Estimation of the errors in the structure factors

For Rietveld and MEM analyses, we use the programs RIETAN-FP [20] and PRIMA [21], respectively. RIETAN-FP estimates the error in the (observed) structure factors as

$$\sigma(|F(\boldsymbol{h}_K)|) = \frac{|F(\boldsymbol{h}_K)|}{2}\left\{\left[\frac{\sigma(I(\boldsymbol{h}_K))}{I(\boldsymbol{h}_K)}\right]^2 + \left[\frac{\sigma(s)}{s}\right]^2\right\}^{1/2} = \frac{|F(\boldsymbol{h}_K)|}{2}\left\{\frac{\Delta 2\theta}{I(\boldsymbol{h}_K)} + \left[\frac{\sigma(s)}{s}\right]^2\right\}^{1/2}, \quad (13)$$

where $I(\boldsymbol{h}_K)$ is the integrated intensity, $\sigma(I(\boldsymbol{h}_K))$ its error based on counting statistics, s the scaling factor in the Rietveld analysis, $\sigma(s)$ its error, and $\Delta 2\theta$ the step width in the measurement [22]. The MEM program PRIMA modifies Eq. (13) as

$$\sigma(|F(\boldsymbol{h}_K)|) = \frac{|F(\boldsymbol{h}_K)|}{2}\left\{\frac{1}{EI(\boldsymbol{h}_K)} + \left[\frac{\sigma(s)}{s}\right]^2\right\}^{1/2} \quad (14)$$

and requires an adjusting factor E to be input [22]. This equation is equivalent to the following equation using an adjusting factor a_E instead of E,

$$\sigma(|F(\boldsymbol{h}_K)|) = \frac{|F(\boldsymbol{h}_K)|}{2}\left\{\frac{(a_E)^2\Delta 2\theta}{I(\boldsymbol{h}_K)} + \left[\frac{\sigma(s)}{s}\right]^2\right\}^{1/2} \quad (15)$$

if we define a_E as $a_E \equiv 1/\sqrt{E\Delta 2\theta}$. The meaning of a_E is simple; it makes the estimated error in the integrated intensity a_E times as large as the purely statistical value. When analyzing the experimentally determined structure factors with PRIMA, the parameter a_E must often be larger than unity to make the calculation converge and to provide a physically reasonable distribution.

2.3. Simulation of (difference) MEM analysis

We simulate the MEM analysis of D_2O-dissolved $BaSn_{0.5}In_{0.5}O_{2.75}$ to examine the effect of the d-spacing cut-off on the spatial resolution of MEM mapping. The simulation procedure is as follows.

First, the diffraction pattern for a model crystal structure is calculated using RIETAN-FP. The maximum count is set to 10^4, a typical value in neutron diffraction experiments. Then the simulated data are analyzed using RIETAN-FP with the scaling factor being the only fitting parameter. The purpose of this procedure is simply to estimate the statistical errors in the structure factors. Finally, the neutron scattering length density distributions are deduced from the structure factors and their errors using MEM for various values of the d-spacing cut-off.

We also simulate the difference MEM analysis of H_2O- and D_2O-dissolved $BaSn_{0.5}In_{0.5}O_{2.75}$ to see how it works. The

simulation procedure is basically the same as described above. The neutron scattering length density distributions are deduced from the differences in the structure factors of H_2O- and D_2O-dissolved $BaSn_{0.5}In_{0.5}O_{2.75}$ and their errors.

3. Experimental methods

3.1. Sample preparation

The $BaSn_{0.5}In_{0.5}O_{2.75}$ samples were prepared by the solid-state reaction of $BaCO_3$ (99.99% pure, Rare Metallic Co., Japan), SnO_2 (99.99% pure, Kojundo Chemical Laboratory Co., Japan), and In_2O_3 (99.99% pure, Rare Metallic Co.) powders. These raw materials were mixed with an agate mortar, pressed into pellets and heated at 1473 K for 20 h in air. They were ground to powder, pressed into pellets again and heated at 1673 K for 40 h in air and for 5 h in dry oxygen flow.

X-ray diffraction (RINT2200, Rigaku Co., Japan) indicated that the final product consisted of a single perovskite phase. Then the $BaSn_{0.5}In_{0.5}O_{2.75}$ powder was heated with a thermobalance at 1273 K in dry oxygen flow to remove absorbed water, and subsequently at 573 K in wet oxygen flow saturated with H_2O vapor at 323 K or D_2O vapor at 327 K. The amount of protium and deuterium uptake into the samples was determined to be 0.3768 H atom and 0.3761 D atom per Ba atom, respectively, assuming the increase in the sample mass to be due solely to the reaction,

$$H_2O+V_O^{\bullet\bullet}+O_O^{\times}\rightarrow 2OH_O^{\bullet}. \quad (16)$$

3.2. Neutron diffraction

The samples were loaded into 10-mm-diameter vanadium cylindrical cells and fixed within aluminum airtight containers for a cryostat in helium atmosphere. Their neutron powder diffraction data were collected at 9 K, with $\Delta 2\theta$ of 0.05°, using high resolution powder diffractometer installed at the Japan Research Reactor 3M of the Japan Atomic Energy Agency. The wavelength of the incident neutrons was 182.3 pm.

4. Results and discussion

4.1. Simulation of (difference) MEM analysis

Figs. 2(a1)–(a3) are isosurface representations of the three-dimensional distribution of the neutron scattering length density in a model structure, i.e., $BaSn_{0.5}In_{0.5}O_{2.75}$-$0.188D_2O$ that has the crystal structure parameters given in Table 1. They have 48 spherical areas at the positions where deuterium atoms have been placed.

Figs. 2(b)–(f) show the distribution $\rho_{2,\mathrm{MEM}}$ deduced by ordinary MEM analysis from the structure factors of the model structure and their simulated errors. When structure factors for a d-spacing larger than 60 pm are used in the MEM analysis, the resulting distribution has 24 bimodal areas around the original deuterium positions. As the d-spacing cut-off increases, the bimodal areas shrink into unimodal areas around the 24l (∼0.07, ∼0.3, 0.5) sites. The areas are then drawn towards the areas attributable to oxygen atoms, and finally merge into them. When the d-spacing cut-off is equal to or greater than 90 pm, the deuterium areas are centered at the 12h (0, ∼0.3, 0.5) sites on the {100} planes, forming lobes of the merged areas. Although the structure considered here is just an example, the above results clearly demonstrate that the spatial resolution of the MEM mapping deteriorates with increasing d-spacing cut-off. In particular, deformation of the deuterium areas is significant probably because they are located close to the oxygen areas, which have much higher scattering length densities.

Figs. 2(g)–(k) show the distribution $\rho_{\mathrm{D,MEM}}$ deduced by difference MEM analysis. It corresponds to the distribution of deuterium atoms alone. More notable are Figs. 2(l)–(p), which show the distribution $\rho_{\mathrm{D,MEM}}+\rho'_{\mathrm{MEM}}$ deduced by combined difference MEM analysis. When the d-spacing cut-off is less than or equal to 80 pm, 24 bimodal areas appear around the original deuterium position. When the d-spacing cut-off is equal to or greater than 90 pm, the deuterium areas connect across the {100} planes. However, even when the d-spacing cut-off is 100 pm, the deuterium areas are clearly separated from the oxygen areas and located mostly off the {100} plane. The combined difference MEM analysis improves the separation between the distributions of atoms, especially of hydrogen and oxygen atoms; it effectively enhances the spatial resolution of MEM mapping.

The above results do not mean that difference MEM analysis is effective only when the d-spacing cut-off is greater than 80 pm. The effectiveness of difference MEM analysis depends on the hydrogen concentration as well as the d-spacing cut-off. Fig. 3 compares the ordinary and difference MEM analyses with a d-spacing cut-off of 60 pm for $BaSn_{0.5}In_{0.5}O_{2.75}$-$0.048D_2O$ that has the same crystal structure as the $BaSn_{0.5}In_{0.5}O_{2.75}$-$0.188D_2O$ except site occupancies. Since the hydrogen concentration is lower and consequently the relative errors in $\Delta F_{\mathrm{D}}(\boldsymbol{h}_K)$ are larger, the maps in Fig. 3 have lower spatial resolution than their counterparts in Fig. 2. In this case, despite the small d-spacing cut-off of 60 pm, the combined difference MEM analysis has definitely higher spatial resolution than the ordinary MEM analysis. Short wavelength neutrons generally improve the spatial resolution of MEM mapping, but yet difference MEM analysis sometimes improves it further.

It should be noted that the tendency of the neighboring areas to connect and merge is common in the ordinary and combined difference MEM analyses. In the combined difference MEM analysis, however, we locate hydrogen atoms and oxygen atoms in separate MEM calculations. In other words, they are not neighboring during the MEM calculations. That seems to be the reason why the combined difference MEM analysis drastically improves the separation between hydrogen and oxygen atoms.

For comparison, we also carry out Fourier synthesis of the structure factors. Figs. 2(q)–(u) show the scattering length density distribution in $BaSn_{0.5}In_{0.5}O_{2.75}$-$0.188D_2O$ obtained from the structure factors $F_2(\boldsymbol{h}_K)$. The termination ripples are so large that they completely mask the distribution attributable to the deuterium atoms. Figs. 2(v)–(z) show the scattering length density distribution of deuterium atoms alone obtained from the difference structure factors $\Delta F_{\mathrm{D}}(\boldsymbol{h}_K)$. The termination ripples diminish and the areas attributable to deuterium atoms are clearly seen in the distribution. These maps are similar to those of difference MEM analysis with larger d-spacing cut-offs. However, calculating the difference in structure factors is not essential in Fourier synthesis because calculating the difference in structure factors followed by Fourier synthesis and calculating the difference in distributions after Fourier synthesis give identical results,

$$\rho_{\mathrm{D,FS}}(\boldsymbol{r},\Delta F_{\mathrm{D}}(\boldsymbol{h}_K))=\frac{b_{\mathrm{D}}[\rho_{2,\mathrm{FS}}(\boldsymbol{r},F_2(\boldsymbol{h}_K))-\rho_{1,\mathrm{FS}}(\boldsymbol{r},F_1(\boldsymbol{h}_K))]}{b_{\mathrm{D}}-b_{\mathrm{H}}}. \quad (17)$$

Here $\rho_{\mathrm{FS}}(\boldsymbol{r},F(\boldsymbol{h}_K))$ is the scattering length density at $\boldsymbol{r}$ Fourier-synthesized from the structure factors $F(\boldsymbol{h}_K)$. It should also be stressed that, unlike the MEM analysis, "combined difference" Fourier synthesis yields the same distribution as ordinary

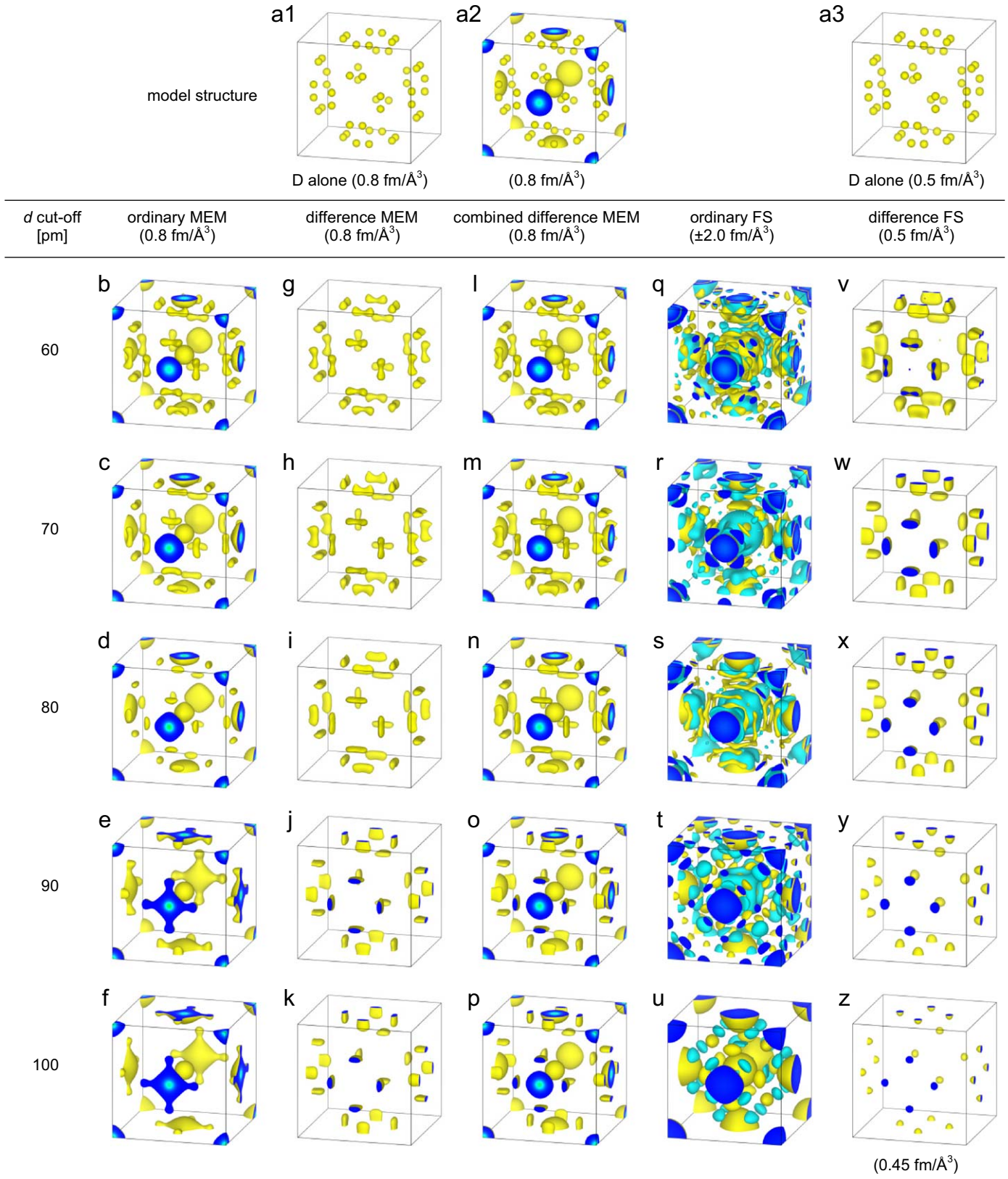

Fig. 2. Simulation of the effect of the *d*-spacing cut-off on the spatial resolution of MEM mapping and Fourier synthesis (FS) mapping for a model structure: $BaSn_{0.5}In_{0.5}O_{2.75}$–$0.188D_2O$ with the structure parameters given in Table 1. Isosurface representations of: (a1)–(a3) the neutron scattering length density distribution in the model structure (isosurfaces at 0.8 or 0.5 fm/Å^3), (b)–(f) the distributions deduced by ordinary MEM analysis for various *d*-spacing cut-offs (0.8 fm/Å^3), (g)–(k) the distributions of deuterium atoms alone deduced by difference MEM analysis (0.8 fm/Å^3), (l)–(p) the distributions corresponding to (b)–(f) deduced by combined difference MEM analysis (0.8 fm/Å^3), (q)–(u) the distributions deduced by FS (±2.0 fm/Å^3), where yellow and cyan surfaces indicate positive and negative areas, respectively, and (v)–(z) the distributions of deuterium atoms alone deduced by difference FS (0.5 fm/Å^3).

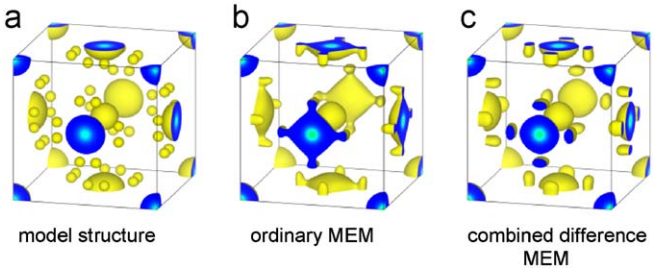

Fig. 3. Comparison of the ordinary and difference MEM analyses with a *d*-spacing cut-off of 60 pm for $BaSn_{0.5}In_{0.5}O_{2.75}-0.048D_2O$; isosurface representations of: (a) the neutron scattering length density distribution in the model structure, (b) the distribution deduced by ordinary MEM analysis, and (c) the distribution deduced by combined difference MEM analysis (isosurfaces at 0.1 fm/Å^3).

Fourier synthesis,

$$\rho_{\mathrm{D,FS}}(\boldsymbol{r}, \Delta F_{\mathrm{D}}(\boldsymbol{h}_K)) + \rho'_{\mathrm{FS}}(\boldsymbol{r}, \Delta F'(\boldsymbol{h}_K)) = \rho_{2,\mathrm{FS}}(\boldsymbol{r}, F_2(\boldsymbol{h}_K)). \quad (18)$$

Thus, it is very difficult to prove or disprove minor distribution of atoms in interstitial regions by Fourier synthesis.

4.2. Analysis of the actual diffraction data

The neutron powder diffraction patterns obtained are shown in Fig. 4. Only reflections allowed by the cubic perovskite structure (space group $Pm\bar{3}m$) were observed. The diffraction angles of the D_2O- and H_2O-dissolved samples were the same, whereas their diffraction intensities were different. Since protium atoms have a large incoherent scattering length, the background for the H_2O-dissolved sample was considerably high.

Another feature of the diffraction patterns was the modulated diffuse background. The standard background function embedded in RIETAN-FP, a finite sum of Legendre polynomials [22], could not reproduce such a complex background satisfactorily. Therefore, we divided the diffraction patterns into three parts, and fit the data for each part separately using RIETAN-FP to estimate the background. We then analyzed all of the data at once, using the composite background function embedded in RIETAN-FP. This function is the product of the estimated background and Legendre polynomials modifying it [22], and could fit the observed background very well.

The results of the Rietveld analysis are summarized in Table 1. For the D_2O-dissolved sample, the refinement located the deuterium atoms at the 48*n* site slightly off the {100} planes. The structure parameters were close to those for D_2O-dissolved $BaSn_{0.5}In_{0.5}O_{2.75+\alpha}$ at 77 K and room temperature [3]. For the H_2O-dissolved sample, on the other hand, the refinement located the protium atoms at the 12*h* site on the {100} planes—even when it was started with protium atoms at the 48*n* site.

The atomic displacement parameters were very large for Ba, Sn/In, and O. Since the measurement temperature was very low (9 K), the large displacement is unlikely to be caused by the thermal vibration or dynamic disorder of constituent atoms. Table 2 summarizes the atomic displacement parameters *U* determined for $BaSn_{1-x}In_xO_{3-x/2}$ and $BaZr_{1-x}In_xO_{3-x/2}$ by neutron powder diffraction. It is seen that indium doping increases all the atomic displacement parameters and that water dissolution further increases the atomic displacement parameters of metal atoms. In these heavily doped and water dissolved perovskite oxides, constituent atoms probably deviate from their normal (averaged) sites because of considerable defects such as dopant atoms, oxygen vacancies and hydrogen atoms. The modulated diffuse backgrounds in the diffraction patterns observed in the present experiment also support the presence of structural disorder.

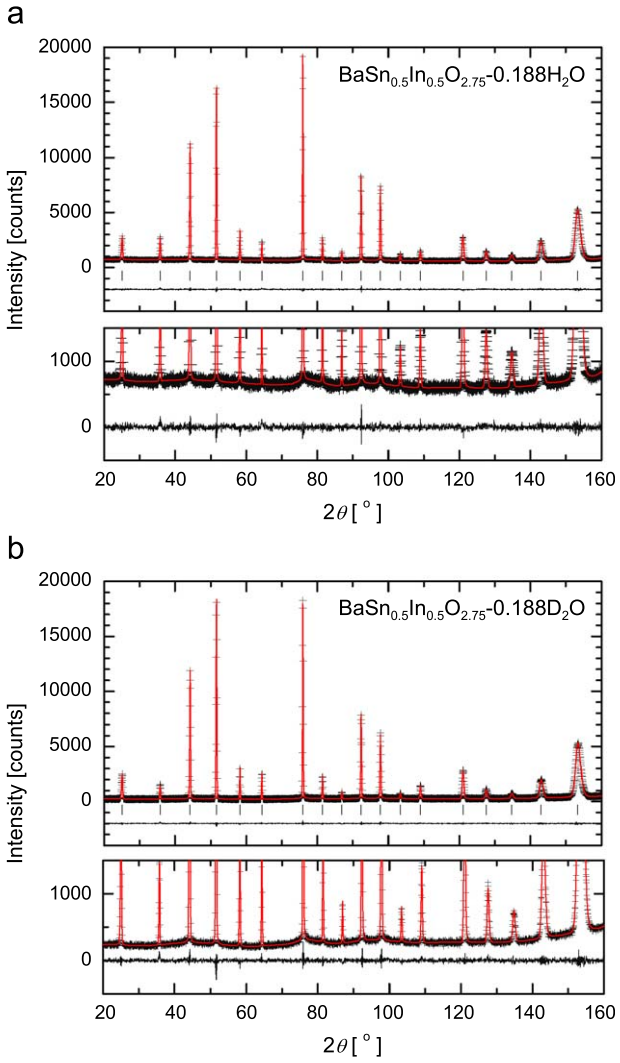

Fig. 4. Neutron diffraction patterns of: (a) $BaSn_{0.5}In_{0.5}O_{2.75}-0.188H_2O$ and (b) $BaSn_{0.5}In_{0.5}O_{2.75}-0.188D_2O$ at 9 K, together with their Rietveld fittings; the lower parts are magnifications of the upper parts. The crosses represent the observed patterns and the upper gray (red) solid lines represent the Rietveld fits to them. The lower solid lines represent the differences between the observed and calculated patterns. The short vertical lines mark the positions of possible Bragg reflections.

It should be reminded here that protium atoms have a coherent neutron scattering cross section only one third of that of deuterium atoms as well as a very large incoherent neutron scattering cross section. These facts mean that the structure parameters of protium atoms determined by the Rietveld analysis are less reliable than those of deuterium atoms. Actually the protium site determined gives an O–H distance of 1.2 Å, which is longer than a typical value (1.0 Å) and might imply that the protium site is erroneous. We therefore cannot conclude that the protium site is really different from the deuterium site.

If, for any reason, the distributions of deuterium and protium atoms are not the same, i.e., $n_{\mathrm{D}}(\boldsymbol{r}) \neq n_{\mathrm{H}}(\boldsymbol{r})$, and the distributions of other atoms are the same, Eq. (4) should be rewritten as

$$\Delta F_{\mathrm{D}}(\boldsymbol{h}_K) = \int_V \left[\frac{b_{\mathrm{D}}(b_{\mathrm{D}} n_{\mathrm{D}}(\boldsymbol{r}) + |b_{\mathrm{H}}| n_{\mathrm{H}}(\boldsymbol{r}))}{b_{\mathrm{D}} + |b_{\mathrm{H}}|}\right] \exp(2\pi \mathrm{i} \boldsymbol{h}_K \cdot \boldsymbol{r})\, \mathrm{d}\boldsymbol{r}. \quad (19)$$

The equation in the square brackets represents the scattering length of deuterium atoms times the weighted arithmetic average of deuterium and protium distributions. On the other hand, Eq. (6)

Table 2
Atomic displacement parameters U of $BaSn_{1-x}In_xO_{3-x/2}$ and $BaZr_{1-x}In_xO_{3-x/2}$ determined by neutron powder diffraction. Note that heavily doped and water dissolved materials have large atomic displacement parameters even at very low temperature.

Material	Temp.	10^2U_{iso}(Ba) (Å^2)		10^2U_{iso}(Sn/In) (Å^2) or 10^2U_{iso}(Zr/In) (Å^2)		10^2U_{11}(O) (Å^2)		10^2U_{33}(O) (Å^2)		10^2U_{iso}(O) (Å^2) or 10^2U_{eq}(O) (Å^2)		Ref.
		Dry	Wet	Dry	Wet	Dry	Wet	Dry	Wet	Dry	Wet	
$BaSnO_3$	RT	0.35(2)	–	0.20(2)	–					0.71(1)	–	[23]
$BaSn_{0.5}In_{0.5}O_{2.75}-0.188H_2O$	9 K	–	1.63(3)	–	0.87(4)	–	2.13(4)	–	1.14(7)	–	1.80(3)	This work
$BaSn_{0.5}In_{0.5}O_{2.75}-0.188D_2O$	9 K	–	1.66(3)	–	0.97(3)	–	2.30(4)	–	1.14(5)	–	1.91(3)	This work
$BaSn_{0.5}In_{0.5}O_{2.75}$ [-0.076D_2O]	10 K	0.66(3)	2.08(6)	0.34(3)	1.03(5)	2.28(4)	2.24(7)	0.55(6)	1.02(8)	1.70(3)	1.83(4)	[2]
$BaSn_{0.5}In_{0.5}O_{2.75}$ [-0.105D_2O]	77 K	0.84(3)	2.01(5)	0.62(3)	1.15(5)	2.51(4)	2.51(7)	0.72(5)	0.86(7)	1.91(3)	1.96(4)	[3]
$BaSn_{0.5}In_{0.5}O_{2.75}$ [-0.105D_2O]	RT	1.27(3)	2.33(6)	0.99(4)	1.38(5)	2.98(4)	2.78(8)	1.08(5)	1.02(7)	2.35(3)	2.19(4)	[3]
$BaSn_{0.5}In_{0.5}O_{2.75}$ [-0.105D_2O]	473 K	1.75(5)	2.82(9)	1.38(5)	2.21(9)	3.60(5)	3.93(10)	1.37(6)	1.63(10)	2.86(3)	3.16(6)	[3]
$BaZrO_3$ [D_2O]	10 K	0.11(4)	0.10(3)	0.18(3)	0.14(3)					0.30(3)	0.33(3)	[24]
$BaZr_{0.75}In_{0.25}O_{2.875}$ [D_2O]	10 K	0.13(4)	0.27(5)	0.24(4)	0.29(4)					0.80(3)	0.71(3)	[24]
$BaZr_{0.50}In_{0.50}O_{2.75}$ [D_2O]	10 K	0.61(8)	1.23(13)	0.54(6)	0.47(11)					1.47(5)	1.48(6)	[24]
$BaZr_{0.5}In_{0.5}O_{2.75}$ [-0.10D_2O]	10 K	0.54(3)	0.85(8)	0.31(3)	0.37(9)	2.30(4)	2.21(12)	0.46(4)	0.15(9)	1.69(2)	1.52(6)	[4]
$BaZr_{0.5}In_{0.5}O_{3-y}$	RT	1.33(4)	–	1.07(3)	–	3.35(4)	–	1.15(6)	–	2.62(3)	–	[6]
$BaZr_{0.5}In_{0.5}O_{2.5}(OD)_x$	5 K	–	1.97(4)	–	1.23(4)	–	3.1(1)	–	1.1(1)	–	2.4(1)	[6]

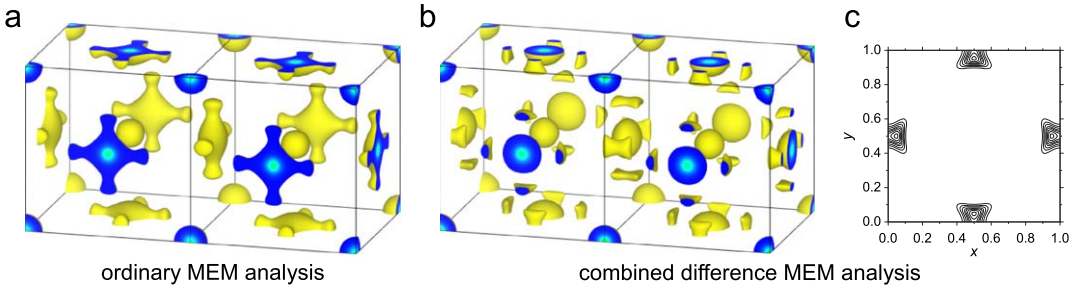

Fig. 5. The neutron scattering length density distributions in $BaSn_{0.5}In_{0.5}O_{2.75}-0.188D_2O$ at 9 K deduced from the observed diffraction data by MEM analysis: (a) three-dimensional isosurface map by ordinary MEM analysis (isosurfaces at 0.8 fm/Å^3), (b) three-dimensional isosurface map by combined difference MEM analysis (isosurfaces at 0.8 fm/Å^3), and (c) two-dimensional contour map at $z = 0.28$ by combined difference MEM analysis (0.25 fm/Å^3 contour interval).

should be rewritten as

$$\Delta F'(\boldsymbol{h}_K) = \int_V \left[\frac{b_D|b_H|(n_D(\boldsymbol{r}) - n_H(\boldsymbol{r}))}{b_D + |b_H|} + \rho'(\boldsymbol{r})\right] \exp(2\pi i \boldsymbol{h}_K \cdot \boldsymbol{r})\, d\boldsymbol{r}. \quad (20)$$

The extra term in the square brackets represents the harmonic average of the scattering lengths times half the difference in deuterium and protium distributions. The difference $n_D(\boldsymbol{r})-n_H(\boldsymbol{r})$ can be negative and thereby the equation in the brackets can also be negative in interstitial regions where $\rho'(\boldsymbol{r})\approx 0$. The program PRIMA can deal with negative distribution correctly only when the distributions of atoms with positive and negative scattering lengths virtually do not overlap with each other [22]. In the present case, the protium distribution is unknown, of course, but it is likely to overlap considerably with the deuterium distribution. Therefore, in the difference MEM analysis, we assumed that the scattering length density for Eq. (20) was positive throughout the unit cell. Note that this assumption prohibits negative areas or protium-dominated areas in the obtained scattering length density distribution.

Finally, we present the neutron scattering length density distribution in $BaSn_{0.5}In_{0.5}O_{2.75}-0.188D_2O$ deduced by MEM analysis; for the analysis, we used the structure factors and the errors in them determined by Rietveld analysis for d-spacing less than 98 nm. Fig. 5(a) shows the distribution obtained by ordinary MEM analysis with an adjusting factor a_E of 1. The areas attributable to deuterium atoms are clearly seen and connected with the areas attributable to oxygen atoms. It appears as if some deuterium and/or oxygen atoms were distributed between their normal sites. On the other hand, Fig. 5(b) shows the distribution obtained by combined difference MEM analysis. Actually we had to set the adjusting factor a_E to 2 for $\sigma_D(|\Delta F_D(\boldsymbol{h}_K)|)$ and 6 for $\sigma'(|\Delta F'(\boldsymbol{h}_K)|)$ to obtain that distribution. This imposed larger errors on the structure factors during the MEM calculation, and should have smoothed out the obtained MEM map to some extent. Nevertheless, the areas attributable to protium/deuterium atoms have their maxima off the {100} planes. These maxima must be due to deuterium atoms because in the preceding Rietveld analyses, the deuterium atoms were located off the {100} planes while the protium atoms were located on the {100} planes. In other words, most of the O–D bonds must tilt towards the second nearest oxygen atoms. Moreover, the areas attributable to protium/deuterium atoms are clearly separated from those attributable to oxygen atoms. The non-zero scattering length densities in the interstitial regions of Fig. 5(a) do not necessarily indicate that deuterium and/or oxygen atoms are located there. More probably, they are artifacts.

Such artifacts or "apparent" atomic distributions can be caused by insufficient spatial resolution of the MEM mapping as demonstrated by the simulation. They are sometimes similar in shape to expected "real" structural disorders, which means that it is not necessarily easy to distinguish between apparent and real distributions. We must be very careful when trying to reveal structural disorder using a MEM map.

5. Conclusions

Difference MEM analysis of the neutron powder diffraction data of H_2O- and D_2O-dissolved $BaSn_{0.5}In_{0.5}O_{2.75}$ indicates that the O–D bonds mostly tilt towards the second nearest oxygen atoms. The large atomic displacement parameters and modulated diffuse background strongly suggest that there is local structural disorder in water-dissolved $BaSn_{0.5}In_{0.5}O_{2.75}$. However, no significant scattering length densities are seen in the interstitial regions of the difference MEM map; the non-zero scattering length densities in the interstitial regions of the ordinary MEM map are probably artifacts.

The present study demonstrates that difference MEM analysis is effective in revealing the structure around hydrogen atoms in that it effectively enhances the spatial resolution of MEM mapping. With diffraction data for shorter wavelength neutrons at elevated temperatures, difference MEM analysis could reveal dynamic disorder and shed some light on the hydrogen diffusion pathways in proton-conducting oxides. In addition, difference MEM analysis can theoretically be applied to other pairs of isotopes although it seems to be most effective for protium and deuterium in oxides because their neutron scattering lengths are considerably different and because the interatomic distances between hydrogen and oxygen are small.

Acknowledgment

This work was partly supported by the 21st Century COE Program "Isotopes for the Prosperous Future."

Appendix A. Supplementary material

Supplementary data associated with this article can be found in the online version at doi:10.1016/j.jssc.2009.06.024.

References

[1] H. Iwahara, Y. Asakura, K. Katahira, M. Tanaka, Solid State Ionics 168 (2004) 299.
[2] T. Ito, T. Nagasaki, K. Iwasaki, M. Yoshino, T. Matsui, N. Igawa, Y. Ishii, Solid State Ionics 178 (2007) 13.
[3] T. Ito, T. Nagasaki, K. Iwasaki, M. Yoshino, T. Matsui, H. Fukazawa, N. Igawa, Y. Ishii, Solid State Ionics 178 (2007) 607.
[4] T. Nagasaki, T. Ito, M. Yoshino, K. Iwasaki, S. Shiotani, H. Fukazawa, N. Igawa, Y. Ishii, J. Nucl. Sci. Technol. Suppl. 6 (2008) 122.
[5] K. Momma, F. Izumi, J. Appl. Crystallogr. 41 (2008) 653.
[6] I. Ahmed, C.S. Knee, M. Karlsson, S.-G. Eriksson, P.F. Henry, A. Matic, D. Engberg, L. Börjesson, J. Alloys Compd. 450 (2008) 103.
[7] E. Kendrick, K.S. Knight, M.S. Islam, P.R. Slater, Solid State Ionics 178 (2007) 943.
[8] A.K. Azad, J.T.S. Irvine, Chem. Mater. 21 (2009) 215.
[9] A. Mitsui, M. Miyayama, H. Yanagida, Solid State Ionics 22 (1987) 213.
[10] R.A. Davies, M.S. Islam, J.D. Gale, Solid State Ionics 126 (1999) 323.
[11] M.S. Islam, R.A. Davies, J.D. Gale, Chem. Mater. 13 (2001) 2049.
[12] M. Yoshino, Y. Liu, K. Tatsumi, I. Tanaka, M. Morinaga, Solid State Ionics 162–163 (2003) 127.
[13] C. Shi, M. Yoshino, M. Morinaga, Solid State Ionics 176 (2005) 1091.
[14] M. Karlsson, M.E. Björketun, P.G. Sundell, A. Maitc, G. Wahnström, D. Engberg, L. Börjesson, I. Ahmed, S. Eriksson, P. Berastegui, Phys. Rev. B 72 (2005) 094303.
[15] M.A. Gomez, M.A. Griffin, S. Jindal, K.D. Rule, V.R. Copper, J. Chem. Phys. 123 (2005) 094703.
[16] M.E. Bjorketun, P.G. Sundell, G. Wahnstrom, Faraday Discuss. 134 (2007) 247.
[17] M. Karlsson, A. Matic, C.S. Knee, I. Ahmed, S.G. Eriksson, L. Börjesson, Chem. Mater. 20 (2008) 3480.
[18] M. Yashima, Solid State Ionics 179 (2008) 797.
[19] K.D. Kreuer, Solid State Ionics 125 (1997) 285.
[20] F. Izumi, K. Momma, Solid State Phenom. 130 (2007) 15.
[21] F. Izumi, R.A. Dilanian, in: S.G. Pandalai (Ed.), Recent Research Developments in Physics Vol. 3, Part II, Transworld Research Network, Trivandrump, 2002, p. 699.
[22] F. Izumi, Multi-purpose pattern-fitting system RIETAN-FP (manual).
[23] E.H. Mountstevens, J.P. Attfield, S.A.T. Redfern, J. Phys.: Condens. Matter 15 (2003) 8315.
[24] I. Ahmed, S.-G. Eriksson, E. Ahlberg, C.S. Knee, M. Karlsson, A. Matic, D. Engberg, L. Börjesson, Solid State Ionics 177 (2006) 2357.